Valley coupling constructed topological two-parameter charge pump

Zixuan Ding,[1] Donghao Wang,[1] Yongchun Tao,[1,*] and Mengyao Li[2,†]
[1]*Department of Physics, Nanjing Normal University, Nanjing 210023, China*
[2]*College of Science, Nanjing Forestry University, Nanjing 210037, Jiangsu, China*

(Received 29 October 2023; accepted 4 December 2023; published 19 December 2023)

Valley coupling is proposed to construct a spatially separated two-parameter pump based on the O- or Y-shaped Kekulé (Kek) graphene superlattices (GSs) with a sandwiched graphene layer. It is shown that for the O-shaped Kek GS pumping structure, pumped charges with an integer number can be obtained in a pumping cycle at the Fermi energy residing in the effective energy gap. Particularly, this quantization only from the contribution of intervalley reflection is thoroughly different from the one in previous two-parameter pumps only with the intravalley reflection. This stems from the Hamiltonian of an antiunitary symmetry, leading to a phase analogous to a topological superconductor and thus a perfect pseudo-Andreev reflection in the valley version. The quantization also can be attributed to the topological interfacial state (TIS) arising in between the two pumping sources due to different quantum valley Hall insulator (QVHI) phases. However, for the Y-shaped Kek GS one, the current coming from both the intravalley and intervalley reflections is nonquantized. This is due to the time-dependent coupling term between two valleys only emerging in the A sublattice, which induces no QVHI and no resultant TISs. Our findings may not only pave a new road to design the quantized charge pump device based on the GS, but also provide a sharp experimental signature to detect the O-shaped one and distinguish between the two GSs.

DOI: 10.1103/PhysRevB.108.245420

I. INTRODUCTION

The quantum parametric pump [1–3] in mesoscopic electron structures, characterizing many-body systems, has been recently attracting extensive interest, particularly thanks to the potential application for realizing novel current standards. In general, it is implemented through two or more time-dependent system parameters with a phase difference, yielding a dc current with no external bias [4,5], which explicitly breaks time-reversal symmetry [6–8]. In particular, a quantized charge pump, in which an integer number of charges can be pumped out during a cycle, has been the principal challenge in this field [9–13].

The most celebrated quantized pump usually refers to the Thouless topological pump (TTP) [4]. Specifically, integral charges can be pumped out by a one-dimensional (1D) moving potential in a cycle at the Fermi energy residing in the energy gap, which is opened by the pumping potential. This 1D periodic system is topological, in which the topological invariant is identical to the pumped charge in each cycle.

The quantum pump has been explored in Dirac systems such as graphene [9,14–16], silicene [17,18], as well as topological insulator [19–21]. For instance, a quantized charge pump based on the pristine graphene can be realized by introducing two staggered potentials [9], whose topological origin is formally different from that of the TTP. Its quantization can be ascribed to the adiabatic evolution of interfacial states born between the two pumping sources, which are topologically protected. However, here we investigate the two-parameter charge pump based on graphene superlattice (GSs) with the valley-related interaction for a Kekulé (Kek) GS.

Electrons in two-dimensional (2D) graphenelike materials, such as graphene, silicene, and transition metal dichalcogenides, possess the extra valley degree of freedom besides the conventional charge and spin counterparts [22–24]. This is because the six corners of the hexagonal Brillouin zone belong to two inequivalent groups, i.e., the so-called K and K' valleys, which leads to the formation of valleytronics [22,25,26]. By inducing the Kek distortion [27–30] or adatom potentials [31,32], several works have been devoted to constructing GSs in order to realize the valley manipulation [32–34]. The GS formed by the periodic lattice distortion, $G = K - K'$, is called the Kek GS [35–37].

The Kek GS has become a promising candidate for valleytronics applications [38,39]. This is because inequivalent K and K' valleys of pristine graphene folded on top of each other can produce nontrivial properties that the pristine graphene does not possess, such as gap opening in the Dirac cone [40–42], valley-momentum locking [30], as well as electron fractionalization [43,44]. For the Kek GS, great advances have been theoretically achieved; meanwhile, it was successfully generated in some experiments based on specific atomic substrates such as Li, Rb, Cs, or Na [45–47]. The valley coupling can be equivalent to an artificial magnetic field [48], and this field can rotate the valley pseudospin as the electron propagates through the GS [32] like the spin rotation by an exchange field in spintronics [49].

*yctao88@163.com
†myli@njnu.edu.cn

 ©2023 American Physical Society

There are two shaped Kek GSs. One is the O-shaped Kek GS [30,44,50], where the carbon-carbon bond strength is altered as in a benzene ring, displaying the property of an opened energy-band gap. The O-shaped Kek GS is now called a valley-version topological insulator. The other is the Y-shaped Kek GS [51] with the honeycomb lattice on a graphene-copper superlattice. In each superlattice unit cell, one of six carbon atoms has no copper atom below it, leading to a shorter nearest-neighbor bond. Several energy band structures have been proposed for the Y-shaped Kek GS, such as two gapless valley bands with valley-momentum locking [29,30], one valley band with a gap opened and the other one with a linear dispersion [33,52], as well as two valley bands with partial gap opening [53]. The Y-shaped Kek GS possessing the third type of band was chosen in this paper. Moreover, the valley coupling in the two Kek GSs can bring about lots of novel physical properties, such as the valley precession [29], valley supercurrent [54], and supercurrent rectification effect [53].

In particular, Beenakker *et al.* [55] showed that the Hamiltonian of the O-shaped Kek GS exhibits an antiunitary symmetry that is formally equivalent to the charge-conjugation symmetry in a superconductor and predicted a valley flip effect via the pseudo-Andreev reflection in a normal G/GS junction. This correspondence leads to the possibility of a phase transition into a phase analogous to a topological superconductor (TSC). Like the Cooper pair potential, the coupling term between the K and K' valleys in the GS behaves as the role of the valley condensation. Thus, the O-shaped Kek GS can be taken as a valley-condensed superconductor. On the other hand, the introduction of the valley coupling in the O-shaped Kek GS can endow the Dirac electrons with a nonzero mass term by opening up an energy gap in the Dirac points. Similar to the staggered potential introduced into graphene, the O-shaped Kek GS actually becomes a quantum valley Hall insulator (QVHI) [56]. However, the experimental evidence of O-shaped Kek GSs is still lacking [52].

Owing to the above-mentioned novel property of the two shaped Kek GSs, naturally, one may ask whether there exist peculiar pumping characteristics such as quantized current when the valley coupling strength is taken as a pumping parameter. This is the main motivation of this paper.

Therefore, we propose a scheme to realize a quantum charge pump based on two O- or Y-shaped Kek GSs and a normal G sandwiched in between them, in which two time-dependent and out-of-phase valley couplings of two GS are taken as pumping parameters, as depicted in Fig. 1(a). By employing lattice and continuum models, respectively, we have obtained the pumping current. It is found that for the O-shaped Kek GS pumping structure, there exists an integer number of electrons pumped out adiabatically in a cycle at the Fermi energy locating in the effective energy gap, which is only provided by the intervalley reflection. This can be explained by the fact that the Hamiltonian with an antiunitary symmetry, formally resembling the charge-conjugate symmetry, leads to a phase analogous to a TSC and a resultant perfect valley flip effect. The quantization could also be ascribed to the adiabatic evolution of the topological interfacial state (TIS) emerging between the two GS regions with different QVHI phases, which is robust against a certain degree of disorders. The

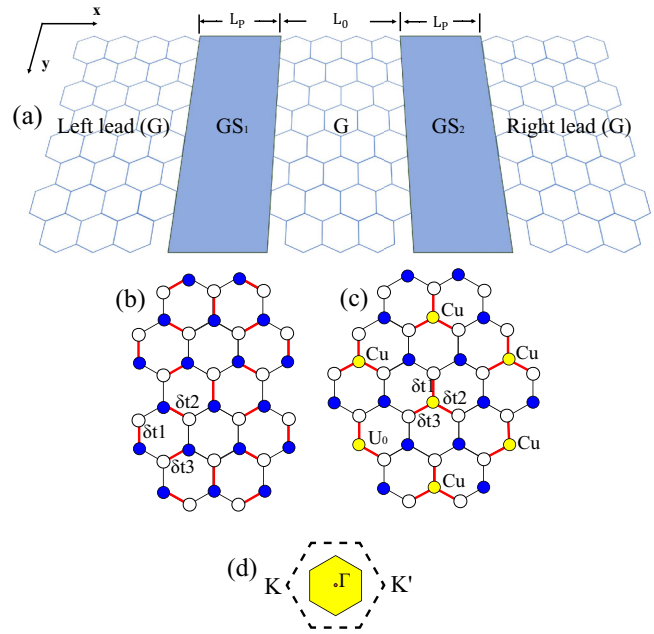

FIG. 1. (a) A schematic sketch of the $G/GS_1/G/GS_2/G$ setup. The coupling strengths $\Delta_{1,2}(t)$ of the $GS_{1,2}$ regions as pumping sources with the length L_P are set as the time-dependent pumping parameters, the length of the middle (sandwiched) G region is L_0, and the left and right G leads are unbiased. In addition, the pumping current direction is assumed along the x axis. (b) The O-shaped Kek GS with the three neighboring-bond modifications δt_i $(i = 1, 2, 3)$ marked by the red solid lines. (c) The Y-shaped Kek GS with the possible site-energy U_0 and neighboring-bond modifications δt_i, in which a substrate atom Cu vacancy (solid yellow circle) in a supercell leads to three contracted neighboring bonds. (d) The two valleys K and K' of the pristine graphene folded into the Γ point of the superlattice Brillouin zone.

quantized current direction is manipulated by such parameters as E, pumping phase φ, and middle or sandwiched G length L_0. However, for the Y-shaped Kek GS pumping structure, the current comes from the intravalley and intervalley reflections, where a quantized platform is not exhibited. Particularly, the current direction is not reversed by adjusting L_0, which is thoroughly different from the O-shaped one. This stems from the time-dependent energy gap controlled by the valley coupling term only emerging at the A sublattice in two Y-shaped Kek GS regions, which cannot generate a topological phase transition, and thus no TIS. Furthermore, the results obtained by the two models are identical in both the O- and Y-shaped pumping structures. Therefore, our findings may shed light on the generation of a quantized charge pump based on the GS and provide an experimental subschema to detect and distinguish Y- and O-shaped Kek GSs.

II. QUANTIZED TWO-PARAMETER PUMP WITH THE O-SHAPED KEK GS

Let us consider a schematic two-parameter pump device shown in Fig. 1(a), where a G layer with the length L_0 is sandwiched in between the two pumping sources $GS_{1,2}$, with $GS_{1,2}$ being, respectively, the left and right GSs, and possible

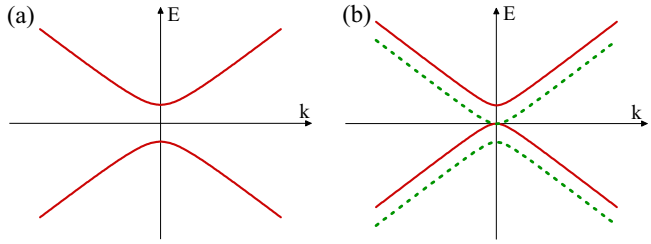

FIG. 2. Electronic band structure $E-k$ of (a) the O-shaped Kek and (b) Y-shaped Kek GSs.

valley currents are pumped into the left or right unbiased G lead. The valley coupling strengths $\Delta_{1,2}(t)$ of $GS_{1,2}$ with the length L_P are taken as time-dependent pumping potentials or parameters. The O-shaped Kek GS is first considered as the pumping source here.

A. Hamiltonian and band structure

First, the O-shaped Kek GS with periodic distortion, which is formed by the contraction of nonadjacent bond lengths between the six carbon atoms of graphene hexagonal lattice, is exhibited in Fig. 1(b). The unit cell is enlarged by $\sqrt{3}\times\sqrt{3}$ and the original K and K' valleys of the pristine graphene are folded into the Γ point [57–59], as shown in Fig. 1(c). Ignoring the complex argument of the valley coupling term, the corresponding low-energy Hamiltonian is given by [30,44]

$$H=\begin{pmatrix} 0 & \hbar v_f k_- & \Delta & 0 \\ \hbar v_f k_+ & 0 & 0 & \Delta \\ \Delta & 0 & 0 & -\hbar v_f k_- \\ 0 & \Delta & -\hbar v_f k_+ & 0 \end{pmatrix}, \tag{1}$$

with $k_\pm = k_x \pm i k_y$, where it acts on the spinor $\Psi = (\Psi_{KA}, \Psi_{KB}, \Psi_{K'A}, \Psi_{K'B})$ containing the sublattice (A and B) and valley (K and K') degrees of freedom of Dirac electrons in graphene with $\hbar v_f = 1$ and momentum $\mathbf{k} = (k_x, k_y)$. The nondiagonal term Δ represents the valley coupling strength, which only stems from the hopping energy modifications of electrons in the honeycomb lattice δt_1, δt_2, and δt_3. In terms of the lattice pseudospin matrix σ_i ($i = x, y, z$) and valley Pauli matrix τ_i, we may rewrite

$$H = \hbar v_f(\sigma_x k_x + \sigma_y k_y)\tau_z + \Delta\tau_x. \tag{2}$$

The Hamiltonian fulfills the time-reversal symmetry, $(\tau_y \otimes \sigma_y)H(\tau_y \otimes \sigma_y) = -H$. If the pumping structure has translational symmetry along the y direction, an additional antiunitary symmetry exists. Particularly, the symmetry is formally equivalent to the charge-conjugation in a superconductor with τ_x switching electron and hole degrees of freedom [55]. This may make the O-shaped Kek GS enter into a phase analogous to a TSC [60,61], where the K and K' valleys correspond to the roles of electron and hole, respectively. The eigenvalue is given by $E_\pm = \pm\sqrt{\Delta^2 + k^2}$, with $k^2 = k_x^2 + k_y^2$, and the corresponding band structure is plotted in Fig. 2(a). It is clearly found that the nonzero valley coupling term can open an energy gap ($2|\Delta|$) in the Dirac point and bring the Dirac electrons with an effective mass. By analogy with the effect of the staggered potential introduced in the pristine graphene, the O-shaped Kek GS actually becomes a QVHI with the nonzero valley Chern number due to the intervalley coupling term [56].

B. Lattice model

Formalism for pumping current. In order to calculate the pumping current, we choose to discretize the real space and transform the above Hamiltonian into a k_y-dependent 1D tight-binding-like model. The following time-dependent quasiclassic Hamiltonian is employed to describe the GS [54],

$$H = \sum_{k_y,j}[C_j^\dagger H_0(k_y)C_j + C_j^\dagger H_x(k_y)C_{j+1} + \text{H.c.}], \tag{3}$$

with the site energy matrix

$$H_0(k_y) = t\sigma_y\tau_z \sin k_y a + (4t_p - 2t_p\cos k_y a)\sigma_z + \Delta_i(t)\tau_x, \tag{4}$$

and hopping matrix

$$H_x(k_y) = -t_p\sigma_z + \mathbb{i}t\sigma_x\tau_z/2, \tag{5}$$

where $C_j^\dagger$ (C_j) is the electron creation (annihilation) operator of the jth site, $t = \hbar v_f/a$ is the hopping energy with lattice constant a, and k_y is the transverse momentum. The valley coupling strengths $\Delta_i(t)$ ($i = 1, 2$) as the time-dependent pumping parameters are given by $\Delta_1(t) = \Delta_0\cos(\omega t)$ and $\Delta_2(t) = \Delta_0\cos(\omega t + \varphi)$ with the pumping strength Δ_0, pumping phase φ, and pumping frequency ω. The t_p term is introduced to remain the single Dirac cone at the band center $k_x = k_y = 0$, but exclude the possible Dirac cone at $k_x = k_y = \pm\pi/a$. Moreover, for pristine graphene, the $\Delta_i(t)$ and t_p terms are not considered. Here, the discretization is just along the x axis; meanwhile, the transverse momentum k_y remains in a continuum form, which means the above Hamiltonian is in a mixed Bloch and lattice model.

The scattering matrix is employed to calculate the pumping current. Based on the lattice Green's function technique, the scattering matrix can be obtained by the Fisher-Lee relation [62],

$$S_{qp}^{\alpha\beta} = -\delta_{\alpha\beta}\delta_{qp} + \mathbb{i}\left[\Gamma_q^\alpha\right]^{1/2} G_{qp}^{\alpha\beta}\left[\Gamma_p^\beta\right]^{1/2}, \tag{6}$$

with $\alpha, \beta \in \{K, K'\}$ indicating the electron in valley K or K' and $p, q \in \{L, R\}$ representing the left and right leads. In Eq. (6), $\Gamma_{q(p)}^{\alpha(\beta)}$ is a block of the linewidth function $\Gamma_{q(p)} = \mathbb{i}(\Sigma_{q(p)}^r - \Sigma_{q(p)}^r)$ with retarded/advanced self-energy $\Sigma_{q(p)}^{r/a}$ calculated numerically by the recursive method and $G_{qp}^{\alpha\beta}$ is the matrix block of the retarded Green's function given by $G^r = [E - H - \Sigma_L^r - \Sigma_R^r]^{-1}$.

The pumping valley-dependent current $I_{L\eta}$ in a period $T = 2\pi/\omega$ is [5]

$$I_{L\eta} = \frac{e}{2\pi T}\int_0^T dt\ \text{Im Tr}\left[\frac{dr_{\eta\eta}}{dt}r_{\eta\eta}^\dagger + \frac{dt'_{\eta\eta}}{dt}t'^\dagger_{\eta\eta} + \frac{dr_{\eta\bar{\eta}}}{dt}r_{\eta\bar{\eta}}^\dagger + \frac{dt'_{\eta\bar{\eta}}}{dt}t'^\dagger_{\eta\bar{\eta}}\right], \tag{7}$$

with $\eta = \pm$ corresponding to K and K', respectively, and $\bar{\eta} = -\eta$. Here, $r_{\eta\eta}$ and $r_{\eta\bar{\eta}}$ are the scattering coefficients of

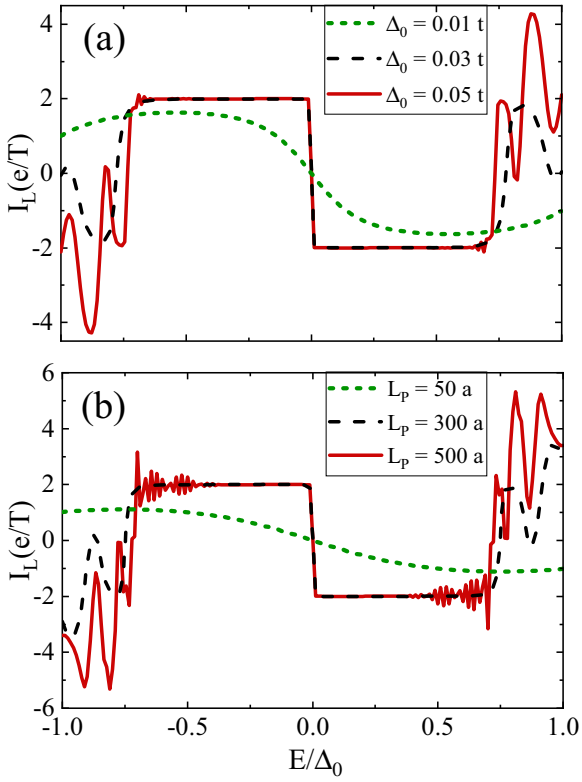

FIG. 3. Pumping charge current I_L as a function of the Fermi energy E with various (a) pumping strength Δ_0 at $L_P = 150a$ and (b) length L_P at $\Delta_0 = 0.02t$. The other parameters are taken as $L_0 = 0$, $k_y = 0$, $t_p = 0.2t$, and $\varphi = 0.5\pi$.

intravalley and intervalley reflections for the injection of electrons from the left lead, respectively, while $t'_{\eta\eta}$ and $t'_{\eta\bar{\eta}}$ are intravalley and intervalley transmissions for the injection of electrons from the right lead, respectively. These scattering coefficients are 2×2 matrices obtained from Eq. (6).

The pumping charge current flowing through the left lead, $I_L = \sum_{\eta=\pm} I_{L\eta}$, is calculated according to Eq. (7), which comes from intervalley and intravalley scattering contributions, written as I_{L1} and I_{L2}, respectively. It is pointed out that the zero temperature (0 K) and adiabatic limit ($\omega \to 0$) are assumed in Eq. (7).

In the calculations, we set the hopping energy $t = 1$ as the energy unit. In this section, it is found that the current $I_{L\eta}$ only includes the contribution from the intervalley reflection $r_{\eta\bar{\eta}}$, which is given by $I_{L\eta} = \frac{e}{2\pi T}\int_0^T dt\ \mathrm{Im\ Tr}[\frac{dr_{\eta\bar{\eta}}}{dt} r^\dagger_{\eta\bar{\eta}}]$ on the basis of Eq. (7), indicating that I_L only includes the contribution I_{L1} from intervalley scattering.

Results and discussions. First, the charge current I_L versus the Fermi energy E with different pumping source length L_P and pumping strength Δ_0 is plotted in Fig. 3. It is clearly seen that for $\Delta_0 = 0.03t$ or $L_P = 200a$, the pumping current shows an obvious quantized platform ($I_L = \pm 2e/T$), in which an integer number of electron charges (2e) are adiabatically pumped out within a pumping cycle. The integer number 2 is related to the valley degeneracy, i.e., the incidence of an electron from the K to K' valley is thoroughly equivalent to that from the K' to K valley by valley coupling. The current fulfills the particle-hole antisymmetric relationship

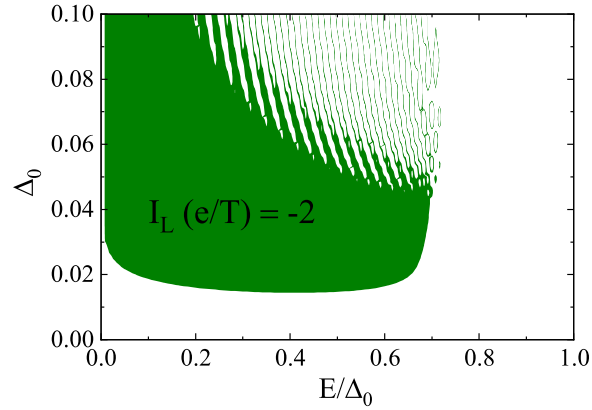

FIG. 4. Pumping charge current I_L in the parameter $(\Delta_0 - E)$ space, where I_L is quantized in the green region while nonquantized outside of it. The other parameters are taken as $L_P = 150a$, $L_0 = 0$, $k_y = 0$, $t_p = 0.2t$, and $\varphi = 0.5\pi$.

$I_L(E) = -I_L(-E)$, a typical property of the two-parameter charge pump device [6].

As usual, the energy range corresponding to the current quantization in Fig. 3(a) is a little smaller than the bulk gap Δ_0 defined for the pristine GS with a uniform and static valley coupling. This is because GS_1 and GS_2 open or close the local energy gap asynchronously with time $\omega t \in (0, T)$ when $\varphi \neq 0$, and thus there exists a nonzero global effective gap approximately given by $E_{ef} = \Delta_0\sqrt{(1-\cos\varphi)/2}$ from Eq. (2). The pumping quantization is jointly tuned by length L_p, strength Δ_0, and Fermi energy E. The quantized platform disappears at a small L_p and Δ_0 due to the quantum tunneling effect. Also, I_L is nonquantized as Δ_0 is large enough, indicating the diminishment of the valley degree of freedom in the two GSs and the absence of TIS.

The quantized-current region in the parameter space $(\Delta_0 - E)$ is presented in Fig. 4, where the green region corresponds to the current value $2e/T$, while I_L is nonquantized in the outside one. The quantized value $I_L = +2e/T$ seems to survive in the case of lower Fermi energy, as shown in Fig. 4, suggesting the evident existence of valley degree. These are much different from those for the previous two-parameter charge pumps in Ref. [9], where the pumping potentials located in the diagonal elements of the Hamiltonian only bring the intravalley reflection.

In addition, when $\Delta_0 = 0.01t$ or $L_P = 50a$, I_L is nonquantized and its maximum will increase with the enhancement of Δ_0 and L_P. The reason is that there exists a finite gap of the TIS caused by the finite-size effect for the smaller Δ_0 and L_P [63]. Thus, with the enhancement of either Δ_0 or L_P, the quantization of I_L is more likely to appear due to the suppressing gap of the TIS. However, for a larger Δ_0 or L_P, the width of the quantized platform of I_L decreases and even vanishes, as shown in Fig. 3 for $\Delta_0 = 0.05t$ or $L_P = 500a$.

We now turn our attention to another important characteristic of the two-parameter pump, i.e., the current-phase relationship shown in Fig. 5(a). It is clearly exhibited that the relationship severely deviates from the sine behavior. Particularly, the quantized platforms with an abrupt current reversal effect between the two quantized values ($+2e/T$ and $-2e/T$)

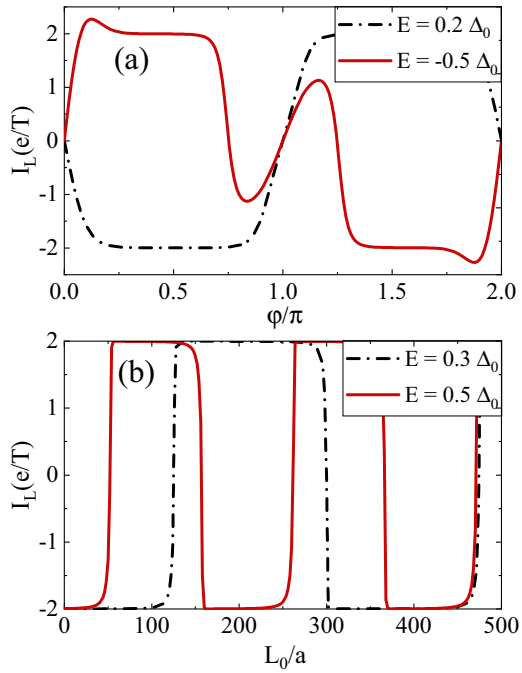

FIG. 5. Pumping charge current I_L as a function of (a) the pumping phase φ at $L_0 = 0$ and (b) the length L_0 at $\varphi = 0.5\pi$. Here, we set $\Delta_0 = 0.03t$, $L_P = 150a$, $t_p = 0.2t$, and $k_y = 0$.

are displayed when $E = 0.2\Delta_0$. Furthermore, only as $\varphi = m\pi$ with an integer m, I_L is not quantized. The reason is that the Fermi energy is easier to reside outside E_{ef} when $\varphi = m\pi$. However, for a larger E, the quantized platform is no longer perfect, accompanied by a pair of peak and valley formed around $\varphi = (2m+1)\pi$ due to the existence of resonance level. The current I_L versus the length L_0 is plotted in Fig. 5(b), reflecting the quantum interference. It exhibits an abrupt variation from the positive quantized value to the negative one, and the reversal period of I_L is decreased with the increasing E, as shown in the previous quantum two-parameter pumps.

As we mentioned earlier, the nonzero valley coupling terms $\Delta_{1,2}(t)$ can open an energy gap in Dirac points and make the pumping sources convert into a topological phase QVHI [56]. The valley Chern number $C_v = \pm 1$ depends on the sign of $\Delta_{1,2}(t)$. The opposite signs for $\Delta_{1,2}(t)$ in the $GS_{1,2}$ regions can produce different quantum phases and there exists a conductive and topologically protected interface connecting the two neighboring phases. Therefore, in the bulk energy gap, the appearance or disappearance of the TIS with ωt exhibits the feature of topological phase transition. In the following, we will account for the topological origin of the pumping quantization through the time-dependent evolution of the TIS bridging the two pumping source regions. The time evolution of the possible interface state in a self-closed system is exhibited in Fig. 6, where the left and right leads are connected to each other. It is shown that two degenerate energy levels either for $E > 0$ or $E < 0$ traverse the energy gap with ωt, which is just the TIS evolution. We can see that the TIS appears in some time intervals, whereas it evolves into the bulk state in other time intervals (see the red solid line in Fig. 6). It follows that charges are shifted from one end to the mid interface and then

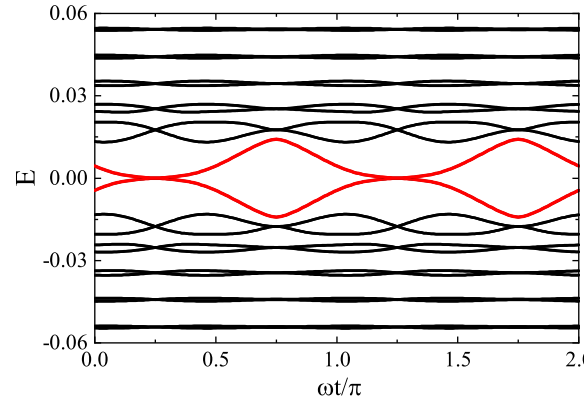

FIG. 6. Adiabatic evolution of the energy band around $E = 0$ with time ωt for a closed system. Here, $L_P = 300a$, $L_0 = 0$, $k_y = 0$, $t_p = 0.2t$, $\Delta_0 = 0.02t$, and $\varphi = 0.5\pi$ are set.

to the other end of the device, just as in the previous quantized two-parameter pumps [9,10].

C. Continuum model

Formalism for pumping current. In this section, we utilize a continuum model to further confirm the above pumping quantization. The proposed $G/GS_1/G/GS_2/G$ junction can be described by the low-energy Dirac Hamiltonian of the form [30,44]

$$H = \hbar v_f(\sigma_x k_x + \sigma_y k_y)\tau_z + \Delta_1(t)\tau_x\Theta_1(x) + \Delta_2(t)\tau_x\Theta_2(x), \tag{8}$$

where τ_i and σ_i (x, y, z) represent the valley and lattice pseudospin Pauli matrices, respectively, the momentum $k_x(k_y) = -\mathrm{i}\partial_x(\partial_y)$, $\Delta_{1,2}(t)$ have been defined above, $\Theta_1(x) = \Theta(x)\Theta(L_P - x)$, and $\Theta_2(x) = \Theta(x - L_0 - L_P)\Theta(2L_P + L_0 - x)$ with $\Theta(x)$ being a Heaviside step function.

By solving Eq. (8), we can obtain the eigenfunctions in each region. The eigenfunctions for the electrons in the K and K' valleys moving along the $\pm x$ direction in each G region are, respectively, given by

$$\begin{aligned}\Psi_G^{K\pm} &= \frac{1}{\sqrt{2}}(1 \quad \pm 1 \quad 0 \quad 0)^T e^{\pm \mathrm{i}k_0 x},\\ \Psi_G^{K'\pm} &= \frac{1}{\sqrt{2}}(0 \quad 0 \quad 1 \quad \mp 1)^T e^{\pm \mathrm{i}k_0 x}.\end{aligned} \tag{9}$$

In each pumping source region, we have the corresponding eigenfunctions,

$$\begin{aligned}\Psi_{GSi}^{K\pm} &= (u_i \quad \pm u_i \quad v_i \quad \pm v_i)^T e^{\pm \mathrm{i}k_i x},\\ \Psi_{GSi}^{K'\pm} &= (v_i \quad \mp v_i \quad u_i \quad \mp u_i)^T e^{\pm \mathrm{i}k_i x},\end{aligned} \tag{10}$$

where $u_{1,2} = \sqrt{\frac{1}{2} + \frac{k_{1,2}}{2E}}$, $v_{1,2} = \sqrt{\frac{1}{2} - \frac{k_{1,2}}{2E}}$, $k_{1,2} = \sqrt{E^2 - \Delta_{1,2}^2(t)}$, and $k_0 = E$ are the wave vectors in the $GS_{1,2}$ and three G regions, respectively.

Consider an incident electron from the K valley of the left lead into GS_1 in Fig. 1(a), where the wave functions in the five different regions are constructed from the linear combination of the corresponding eigenfunctions, respectively, which are

written as

$$\begin{aligned}
\Psi_I &= \Psi_G^{K+} + r_{KK}\Psi_G^{K-} + r_{K'K}\Psi_G^{K'-},\\
\Psi_{II} &= a_1\Psi_{GS_1}^{K+} + b_1\Psi_{GS_1}^{K-} + c_1\Psi_{GS_1}^{K'+} + d_1\Psi_{GS_1}^{K'-},\\
\Psi_{III} &= e\Psi_G^{K+} + f\Psi_G^{K-} + g\Psi_G^{K'+} + h\Psi_G^{K'-},\\
\Psi_{IV} &= a_2\Psi_{GS_2}^{K+} + b_2\Psi_{GS_2}^{K-} + c_2\Psi_{GS_2}^{K'+} + d_2\Psi_{GS_2}^{K'-},\\
\Psi_V &= t_{KK}\Psi_G^{K+} + t_{K'K}\Psi_G^{K'+},
\end{aligned} \tag{11}$$

where $\Psi_i (i = I \sim V)$ are the wave functions in the left lead, GS_1, middle G, GS_2, and right lead, respectively. r_{KK}, $r_{K'K}$, t_{KK}, and $t_{K'K}$ correspond to the intravalley reflection, intervalley reflection, intravalley transmission, and intervalley transmission coefficients, respectively. Moreover, $r_{K'K}$ and $t_{K'K}$, describing the valley flip effects at the two interfaces, are analogous to the local and nonlocal Andreev reflections in the normal metal/superconductor junction, respectively. This is because the Hamiltonian has the same antiunitary symmetry as in a superconductor, as mentioned above. Therefore, the valley flip effect with nonzero $r_{K'K}$ is also termed the valley pseudo-Andreev reflection. By using the boundary conditions at the four interfaces,

$$\begin{aligned}
&\Psi_I|_{x=0} = \Psi_{II}|_{x=0},\\
&\Psi_{II}|_{x=L_P} = \Psi_{III}|_{x=L_P},\\
&\Psi_{III}|_{x=L_P+L_0} = \Psi_{IV}|_{x=L_P+L_0},\\
&\Psi_{IV}|_{x=2L_P+L_0} = \Psi_V|_{x=2L_P+L_0},
\end{aligned} \tag{12}$$

a set of 16 linearly independent equations are yielded. Solving these equations, we can attain the following scattering coefficients:

$$\begin{aligned}
r_{K'K} &= r_1 + \frac{e^{\mathrm{i}\varphi_0}t_1^2 r_2}{1 - e^{\mathrm{i}\varphi_0}r_1 r_2},\\
t_{KK} &= \frac{e^{-2\mathrm{i}k_0 L_P}t_1 t_2}{1 - e^{\mathrm{i}\varphi_0}r_1 r_2},\\
r_{KK} &= 0,\\
t_{K'K} &= 0,
\end{aligned} \tag{13}$$

where $r_i = \Delta_i(t)(1 - e^{2\mathrm{i}k_i L_P})/[(E + k_i) - e^{2\mathrm{i}k_i L_P}(E - k_i)]$, $t_i = 2k_i e^{\mathrm{i}k_i L_P}/[(E + k_i) - e^{2\mathrm{i}k_i L_P}(E - k_i)]$, and $\varphi_0 = 2k_x L_0$. Due to valley degeneracy, the situation for the incident electron from the K' valley owns the same value of corresponding scattering coefficients. In addition, the transmission coefficient for the incident electron from the left lead is equal to that from the right lead.

From Eq. (13), we can infer the scattering coefficients $r_{\eta\eta}$ and $t'_{\eta\bar{\eta}}$ are thoroughly prohibited ($\eta, \bar{\eta}$ defined above), thus, according to Eq. (7), the current formula can be rewritten as

$$I_{L\eta} = \frac{e}{2\pi T}\int_0^T dt\ \mathrm{Im}\left[\frac{dr_{\eta\bar{\eta}}}{dt}r^*_{\eta\bar{\eta}} + \frac{dt'_{\eta\eta}}{dt}t'^*_{\eta\eta}\right], \tag{14}$$

with $r_{\eta\bar{\eta}}$ for the incident electron from the left lead and $t'_{\eta\eta}$ for the incident one from the right lead. We find that when the $E < E_{ef}$, the $|t'_{\eta\eta}|^2$ will vanish but the $|r_{\eta\bar{\eta}}|^2 = 1$, and thus only the reflection coefficient $r_{\eta\bar{\eta}}$ dose contributes to the pumping current. This is consistent with the previous result by the lattice model.

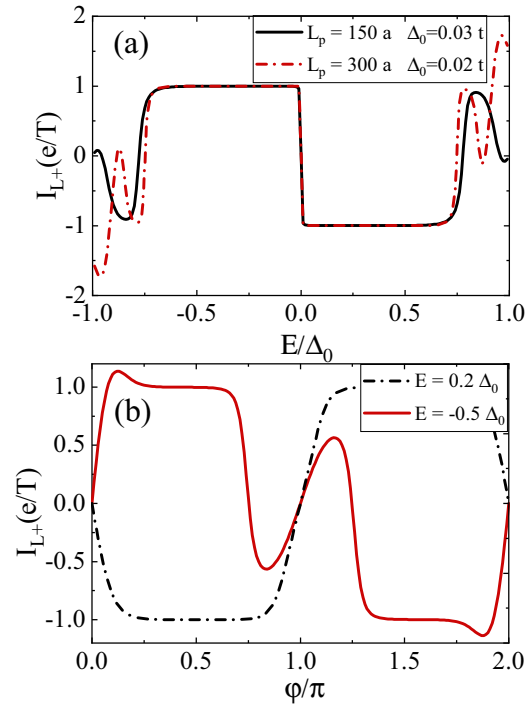

FIG. 7. Pumping current I_{L+} as a function of (a) the energy E at $\varphi = 0.5\pi$ and (b) the pumping phase φ at $L_P = 150a$ and $\Delta_0 = 0.03t$. The other parameters are $t_p = 0.2t$, $L_0 = 0$, and $k_y = 0$.

Results and discussions. We plot I_{L+} versus E and φ in Figs. 7(a) and 7(b), respectively, which shows the quantized platform. Because of valley degeneracy, I_{L-} possesses the same value with I_{L+}. Therefore, the features we obtained have no difference from those shown in Figs. 3 and 5(a), respectively. Particularly, the pumping current could be quantized only if E resides in E_{ef}. It could be inferred that the bulk states should almost have a negligible influence on the quantized I_L because of $t'_{\eta\eta} = 0$ being a precondition of the results shown in Fig. 7.

Owing to $|r_{\eta\bar{\eta}}|^2 = 1$, the pumped charge in a period T is equal to the winding number of the reflection coefficient $r_{\eta\bar{\eta}}$, $\omega = \frac{1}{2\pi\mathrm{i}}\oint r^*_{\eta\bar{\eta}}dr_{\eta\bar{\eta}}$. To understand the quantized pump further, we also exhibit the argument θ of reflection coefficient r_{+-} as a function of ωt and its trace in the complex plane for the different Fermi energy E in Fig. 8. When the pumping current is quantized at $E = 0.2\Delta_0$, $\theta(\omega t)$ experiences a jump of 2π in a cycle and the orbit of r_{+-} is a unit circle in the complex plane, as shown in Figs. 8(a) and 8(b), respectively. However, for the nonquantized pumping current at $E = 0.8\Delta_0$, a different situation appears in Figs. 8(c) and 8(d), where a rapid jump of 2π is not exhibited for $\theta(\omega t)$ and thus its orbit is far away from experiencing a circle. The trace is a closed circle owing to the Hamiltonian being periodic and keeping invariant as long as $E < E_{ef}$, which implies the winding of r_{+-} being a unit of ± 1 and resultantly a unit of charge pumped out in a cycle. Similarly, because of the valley degeneracy involved in transport, the same situation is for r_{-+}.

As demonstrated in Ref. [55], there exists a complete valley switch in the O-shaped Kek GS. An incident electron in the valley K is thoroughly reflected in the other valley K',

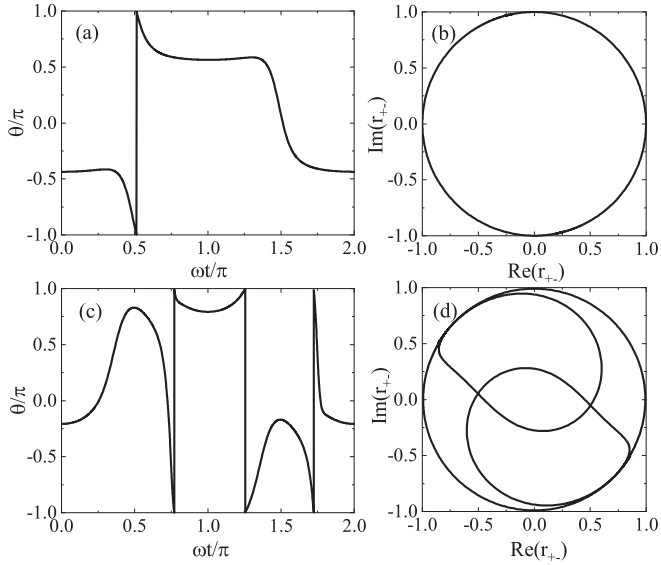

FIG. 8. The argument θ of reflection coefficient r_{+-} evolves with time $\omega\tau$ in the (a) for $E = 0.2\Delta_0$ and (c) for $E = 0.8\Delta_0$, and the corresponding trace in the complex plane is plotted in (b) and (d), respectively. The other parameters are the same as that of the red line in Fig. 7(a).

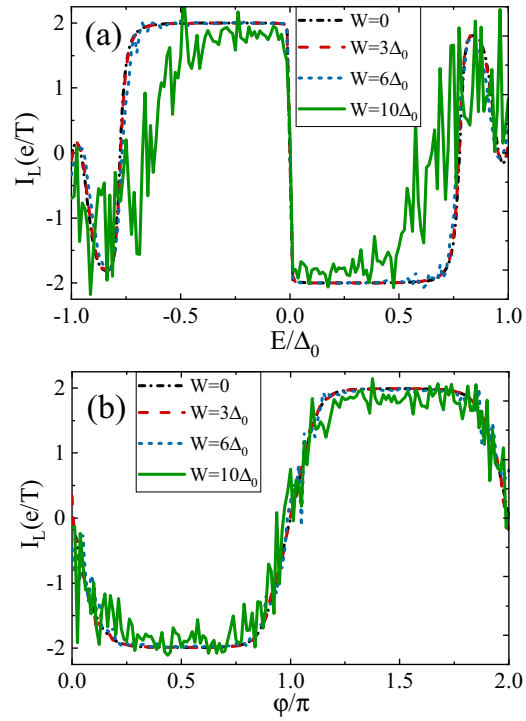

FIG. 9. The current I_L as functions of (a) E and (b) φ for various disorder strengths W. The other parameters are the same as those corresponding to the black line in Fig. 7.

which leads to the quantized current obtained in our pumping structure. This intervalley reflection with $|r_{\eta\bar{\eta}}|^2 = 1$ is protected by a topological invariant named the Pfaffian invariant [64], which resembles the complete Andreev reflection from a Majorana zero mode. As a result, the quantized I_L is also topologically protected. In Fig. 9, we confirm the robustness of the quantized current to disorder and plot I_L versus E and φ with different disorder strength W. This disorder is modeled by the random on-site potential $H_d = \sum_i v_i$, where v_i is the random potential uniformly distributed in the interval $[-W, W]$. It is found that the quantized I_L can survive in the weak and moderate disorders, such as $W = 3\Delta_0$ and $6\Delta_0$. However, the quantization will be destroyed in E_{ef} for the stronger disorder $W = 10\Delta_0$. Therefore, the quantization is robust against nonmagnetic disorders due to the topological property of the O-shaped Kek GS.

III. TWO-PARAMETER PUMP WITH THE Y-SHAPED KEK GS

A. Hamiltonian and band structure

In this section, we turn our attention to the charge pump based on the Y-shaped Kek GS, as shown in Fig. 1(a). The Y-shaped Kek GS with one of six carbon atoms in each superlattice unit cell deposited on the substrate-atom (Cu) vacancy, as exhibited in Fig. 1(c), induces a shorter nearest-neighbor bond. In spite of modifications of both the hopping energy of electrons and site energy of the carbon atom in relation to the Cu vacancy, we only consider the site-energy modification ($U_0 \neq 0$) in the following Hamiltonian for simplicity. The unit cell enlarged by $\sqrt{3} \times \sqrt{3}$ also folds and couples the original two valleys into the same Γ point, as shown in Fig. 1(d). The corresponding low-energy Hamiltonian [29], being the same as that of the periodic adatoms-modified graphene studied in Ref. [31], is written as

$$H = \hbar v_f(\tau_z\sigma_x k_x + \sigma_y k_y) + \frac{\Delta}{2}(\sigma_0 + \sigma_z)\tau_x, \tag{15}$$

where the second term represents the valley coupling effect with strength Δ, as in Eq. (2), fulfilling the time-reversal symmetry. Notedly, a coupling or a "chiral" coupling term between the K and K' valleys only occurs at the A sublattice in the Hamiltonian. The eigenvalues are simply given by $E_\pm = \pm\frac{\Delta}{2} \pm \sqrt{(\frac{\Delta}{2})^2 + k^2}$, with $k^2 = k_x^2 + k_y^2$. The corresponding band structure is shown in Fig. 2(b), where the valence or conduction band in the two valley-helical energy bands has moved up or down by the magnitude $|\Delta|$. This means the bands open up only a half gap, compared with the O-shaped Kek GS shown in Fig. 2(a).

B. Lattice model

Formalism of the pumping current. By using the lattice Green's function method, we calculate the pumping current and the quasiclassic Hamiltonian reads as [53]

$$H = \sum_{k_y, j}[C_j^+ H_0(k_y)C_j + C_j^+ H_x(k_y)C_{j+1} + \text{H.c.}], \tag{16}$$

with the site-energy matrix

$$H_0(k_y) = t\sigma_y \sin k_y a + (4t_p - 2t_p \cos k_y a)\sigma_z + \Delta_i(t)(\sigma_0 + \sigma_z)\tau_x, \tag{17}$$

and hopping matrix

$$H_x(k_y) = -t_p\sigma_z - \mathbb{i}t\sigma_x\tau_z/2. \tag{18}$$

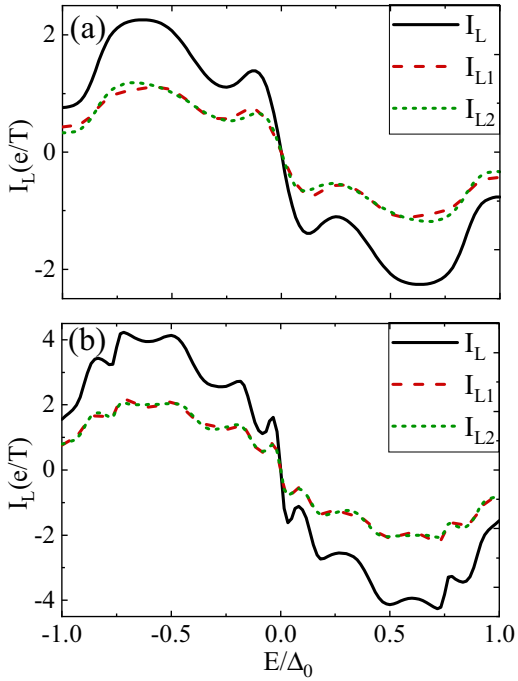

FIG. 10. Pumping charge current I_L, I_{L1}, and I_{L2} as a function of the Fermi energy E with (a) $\Delta_0 = 0.01t$ and (b) $0.02t$. Here, we set $t_p = 0.02t$, $L_P = 400a$, $k_y = 0$, $L_0 = 0$, and $\varphi = 0.5\pi$.

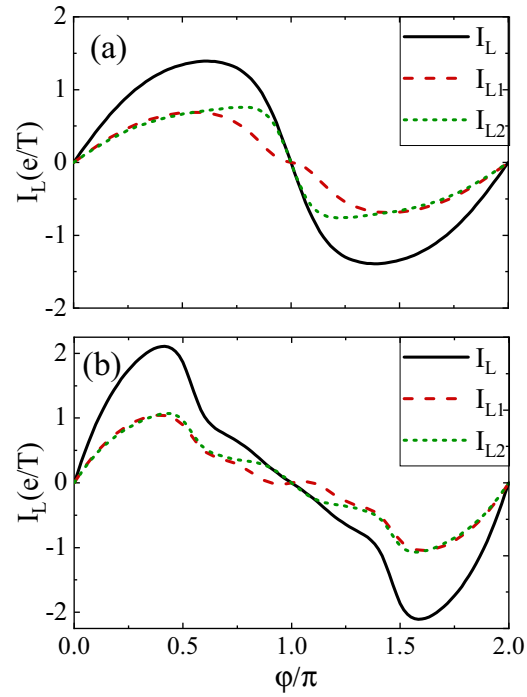

FIG. 11. Pumping charge current I_L, I_{L1}, and I_{L2} vs the pumping phase φ with (a) $E = -0.1\Delta_0$ and (b) $-0.8\Delta_0$. The other parameters are the same as in Fig. 10(a).

Particularly, we can find that the current $I_{L\eta}$ stems from the contributions of both $r_{\eta\eta}$ and $r_{\eta\bar{\eta}}$, which are given by $I_L^{r_{\eta\eta}} = \frac{e}{2\pi T}\int_0^T dt\ \mathrm{Im\ Tr}[\frac{dr_{\eta\eta}}{dt} r_{\eta\eta}^\dagger]$ and $I_L^{r_{\eta\bar{\eta}}} = \frac{e}{2\pi T}\int_0^T dt\ \mathrm{Im\ Tr}[\frac{dr_{\eta\bar{\eta}}}{dt} r_{\eta\bar{\eta}}^\dagger]$ on the basis of Eq. (7), respectively. This indicates that I_L comes from the contributions of both the intervalley and intravalley reflections, namely, I_{L1} and I_{L2}.

Results and discussions. First, we present the pumping currents I_L, I_{L1}, and I_{L2} as a function of E under different Δ_0 in Fig. 10. Similarly, it is found that $I_L = 2I_{L\eta}$ due to the valley degeneracy $I_{L\eta} = I_{L\bar{\eta}}$ and still satisfies $I_L(E) = -I_L(-E)$. Although the currents I_L, I_{L1}, and I_{L2} do not show a quantized platform, they can reach very sizable values. The absence of a quantized platform is an important difference from that for the pump device based on the O-shaped Kek GS. Obviously, I_{L1} is almost equal to I_{L2} all the time. With the enhancement of E from $-\Delta_0$ to 0, the currents, which are always greater than 0, first increase and then decrease with a trend toward zero, accompanied by slight fluctuations. The larger Δ_0 is, the more frequently the currents fluctuate. In addition, with Δ_0 increased, the maximum of currents is larger, such as the maximum of I_L exceeds $4e/T$ at $\Delta_0 = 0.02t$ shown in Fig. 10(b).

Next, we investigate the variation of I_L, I_{L1}, and I_{L2} with φ under different E, as illustrated in Fig. 11. It is clearly exhibited that the currents still deviate from the sine behavior; however, they do not show a quantized platform. Around $\varphi \sim (2m+1)\pi$, there exists a significant difference between I_{L1} and I_{L2}. For a larger E, I_{L1} and I_{L2} have clear fluctuations due to the existence of resonance level. Additionally, the currents I_L, I_{L1}, and I_{L2} versus the length L_0 with different E are plotted in Fig. 12. It is found that I_L, I_{L1}, and I_{L2} show an oscillatory behavior with same period. Particularly, their period decreases with the enhancement of E, which is similar to the features of I_L versus L_0 for the O-shaped Kek GS pump shown in Fig. 5(b). For a small E, $I_{L1} \approx I_{L2}$. Moreover, when E increases, the amplitude of I_{L2} gets less than the that of

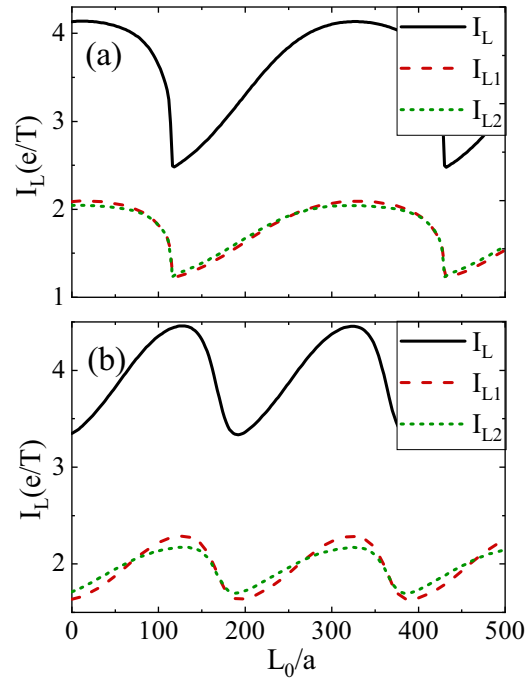

FIG. 12. Pumping charge current I_L, I_{L1}, and I_{L2} vs the length L_0 with (a) $E = -0.3\Delta_0$ and (b) $-0.5\Delta_0$. The other parameters are the same as in Fig. 10(b).

I_{L1}. In addition, the sign of current is unchanged all the time, meaning that the reversal effect of the current direction is not realized by L_0.

The features obtained by using lattice and continuum models have been verified in the previous section, so we do not discuss the continuum model here for simplicity. Now, we explore the reason why the quantized current cannot be realized in the Y-shaped Kek GS pumping structure. As we discussed earlier, for the O-shaped Kek GS, the pumping quantization could be attributed to the evolution of the TIS bridging the two pumping sources. Notedly, the valley coupling terms at both A and B sublattices in the Hamiltonian open up a complete energy gap $2|\Delta_{1(2)}|$. As a result, the GS can enter into the QVHI phase. However, for the energy band of the Y-shaped Kek GS shown in Fig. 2(b), it exhibits the two valley bands with a partially opened gap $|\Delta_{1(2)}|$ due to the coupling valley term only at the A sublattice. The energy gap controlled by the corresponding time-dependent valley coupling term in the two GS regions cannot lead to a quantum phase transition; thus, there is no TIS forming in the O-shaped Kek GS pumping structure. Therefore, the different valley coupling effects in the Hamiltonian bring essential differences between the Y- and O-shaped Kek GSs, which are responsible for the unique pumping characteristics, respectively.

IV. EXPERIMENTAL ACCESSIBILITY ANALYSIS

We have discussed the proposed two-parameter charge pump devices based on the two Kek GSs. Two energy-band gaps of O-shaped Kek GS are completely opened, whereas the gaps of Y-shaped Kek GS are partially opened. Experimentally, Gutierrez *et al.* [51] have successfully imaged the Y-shaped Kek distortion in graphene grown on a Cu(111) surface. The copper vacancies on Cu(111), bringing the modulations of both the Y-shaped hopping energy and original site energy, lead to the occurrence of Y-shaped Kek GS. Bao *et al.* [36] reported experimentally that intercalating Li atoms between graphene sheets and an SiC substrate will form a Kek superlattice structure. Their work first demonstrated the O-shaped Kek modulation and showed that it exists only near the gap edge of the Dirac cone. The successful exploration offers a good experimental basis for our structure based on O-shaped Kek GS. In addition, the above-mentioned Hamiltonians in the present work can also be used to describe the periodic adatom-graphene superlattice [31], where the same valley coupling term Δ will be controlled by the different site-energy modifications of electrons.

V. CONCLUSIONS

In summary, by using lattice and continuum models, we have investigated a possible quantized pump based on a $G/GS_1/G/GS_2/G$ junction with the O- or Y-shaped Kek GSs, in which two time-dependent and out-of-phase valley couplings in two GS regions are taken as pumping parameters. Four features are exhibited as follows. For the O-shaped Kek GS, (1) a possible quantized noiseless charge current is obtained at E lying in the effective energy gap E_{ef}, coming from the intervalley reflection, and (2) its direction can be reversed abruptly by the sandwiched G length L_0. However, for the Y-shaped one, (1) the current does not show a quantized platform, which comes from both the intravalley and intervalley reflections, and (2) its direction cannot be modulated by L_0.

Physically, the unique pumping characteristics of the O- and Y-shaped Kek GS pumping structures originate from the different corresponding Hamiltonian due to different valley coupling, respectively. For the former, the intervalley reflection-induced quantization can be deemed as a pseudo-Andreev reflection of the valley version with unity, which stems from the Hamiltonian of an antiunitary symmetry, leading to a phase being analogous to a topological superconductor. The quantization also can be ascribed to the TIS born in between the two pumping sources due to the different quantum valley Hall phases. For the latter, the absence of TISs is because the time-dependent energy gap controlled by the coupling valley term only appearing at A sublattices in two GS regions, which cannot generate a quantum phase transition.

Currently, the experimental study of the Kek GS, particularly the O-shaped one, is still in its early stage, although some achievements have been made [36,51,52]. Therefore, our findings may pave a new way to fabricate a different pump device based on GSs and afford a different scheme to experimentally detect the O-shaped Kek GS and distinguish between the two GSs.

ACKNOWLEDGMENTS

The authors would like to thank Prof. Jun Wang of Southeast University for the tremendous help. This work was supported by the National Natural Science Foundation of China (Grant No. 12274232).

[1] B. Spivak, F. Zhou, and M. T. Beal Monod, Mesoscopic mechanisms of the photovoltaic effect and microwave absorption in granular metals, Phys. Rev. B **51**, 13226 (1995).

[2] M. Switkes, C. M. Marcus, K. Campman, and A. C. Gossard, An adiabatic quantum electron pump, Science **283**, 1905 (1999).

[3] P. W. Brouwer, Scattering approach to parametric pumping, Phys. Rev. B **58**, R10135 (1998).

[4] D. J. Thouless, Quantization of particle transport, Phys. Rev. B **27**, 6083 (1983).

[5] M. Böttiker, H. Thomas, and A. Prêtre, Current partition in multiprobe conductors in the presence of slowly oscillating external potentials, Z. Phys. B **94**, 133 (1994).

[6] M. Moskalets and M. Büttiker, Floquet scattering theory of quantum pumps, Phys. Rev. B **66**, 205320 (2002).

[7] M. Moskalets and M. Büttiker, Adiabatic quantum pump in the presence of external ac voltages, Phys. Rev. B **69**, 205316 (2004).

[8] A. Kundu, S. Rao, and A. Saha, Quantum charge pumping through a superconducting double barrier structure in graphene, Phys. Rev. B **83**, 165451 (2011).

[9] J. Wang and J.-F. Liu, Quantized charge pump of massive Dirac electrons, Phys. Rev. B **95**, 205433 (2017).

[10] J. Wang, J. F. Liu, and C. S. Ting, Topological two-parameter charge pump in a one-dimensional semiconductor nanowire superlattice, Phys. Rev. B **100**, 075402 (2019).

[11] X.-H. Wang, J. J. Wang, J. Wang, and J.-F. Liu, Flat band assisted topological charge pump in the dice lattice, Phys. Rev. B **103**, 195442 (2021).

[12] H. Tan, P.-H. Fu, Y.-R. Chen, J.-F. Liu, J. Wang, and Z. Ma, Quantized Majorana pump in semiconductor-superconductor heterostructures, Phys. Rev. B **103**, 195407 (2021).

[13] V. F. Becerra, M. Trif, and T. Hyart, Quantized spin pumping in topological ferromagnetic-superconducting nanowires, Phys. Rev. Lett. **130**, 237002 (2023).

[14] M. J. Wang, J. Wang, and J. F. Liu, Efficient charge pump by pure mechanical resonators in graphene, Europhys. Lett. **121**, 47002 (2018).

[15] M.-J. Wang, J. Wang, and J.-F. Liu, Possible quantized charge pump in bilayer and trilayer graphene, New J. Phys. **22**, 013042 (2020).

[16] E. Prada, P. San-Jose, and H. Schomerus, Quantum pumping in graphene, Phys. Rev. B **80**, 245414 (2009).

[17] G. C. Paul and A. Saha, Quantum charge pumping through resonant crossed Andreev reflection in a superconducting hybrid junction of silicene, Phys. Rev. B **95**, 045420 (2017).

[18] J. T. J. Marcellino, M.-J. Wang, and S. K. Wang, Generation of valley pump currents in silicene, Chin. Phys. B **28**, 017204 (2019).

[19] M. Kawamura, M. Mogi, R. Yoshimi, T. Morimoto, K. S. Takahashi, A. Tsukazaki, N. Nagaosa, M. Kawasaki, and Y. Tokura, Laughlin charge pumping in a quantum anomalous Hall insulator, Nat. Phys. **19**, 333 (2023).

[20] P. Zhu, A. Alexandradinata, and T. L. Hughes, $\mathbb{Z}_2$ spin Hopf insulator: Helical hinge states and returning Thouless pump, Phys. Rev. B **107**, 115159 (2023).

[21] B.-L. Wu, A.-M. Guo, Z.-Q. Zhang, and H. Jiang, Quantized charge-pumping in higher-order topological insulators, Phys. Rev. B **106**, 165401 (2022).

[22] D. Xiao, W. Yao, and Q. Niu, Valley-contrasting physics in graphene: Magnetic moment and topological transport, Phys. Rev. Lett. **99**, 236809 (2007).

[23] F. Zhai, X. Zhao, K. Chang, and H. Q. Xu, Magnetic barrier on strained graphene: A possible valley filter, Phys. Rev. B **82**, 115442 (2010).

[24] D. Gunlycke and C. T. White, Graphene valley filter using a line defect, Phys. Rev. Lett. **106**, 136806 (2011).

[25] A. R. Akhmerov, J. H. Bardarson, A. Rycerz, and C. W. J. Beenakker, Theory of the valley-valve effect in graphene nanoribbons, Phys. Rev. B **77**, 205416 (2008).

[26] O. Gunawan, Y. P. Shkolnikov, K. Vakili, T. Gokmen, E. P. De Poortere, and M. Shayegan, Valley susceptibility of an interacting two-dimensional electron system, Phys. Rev. Lett. **97**, 186404 (2006).

[27] D. A. Ruiz-Tijerina, E. Andrade, R. Carrillo-Bastos, F. Mireles, and G. G. Naumis, Multiflavor dirac fermions in Kekulé-distorted graphene bilayers, Phys. Rev. B **100**, 075431 (2019).

[28] P. Gao, D. Torrent, F. Cervera, P. San-Jose, J. Sánchez-Dehesa, and J. Christensen, Majorana-like zero modes in Kekulé distorted sonic lattices, Phys. Rev. Lett. **123**, 196601 (2019).

[29] J. J. Wang, S. Liu, J. Wang, and J.-F. Liu, Valley-coupled transport in graphene with Y-shaped Kekulé structure, Phys. Rev. B **98**, 195436 (2018).

[30] O. V. Gamayun, V. P. Ostroukh, N. V. Gnezdilov, I. Adagideli, and C. W. J. Beenakker, Valley-momentum locking in a graphene superlattice with Y-shaped Kekulé bond texture, New J. Phys. **20**, 023016 (2018).

[31] Y. Ren, X. Deng, Z. Qiao, C. Li, J. Jung, C. Zeng, Z. Zhang, and Q. Niu, Single-valley engineering in graphene superlattices, Phys. Rev. B **91**, 245415 (2015).

[32] S. K. Wang and J. Wang, Valley precession in graphene superlattices, Phys. Rev. B **92**, 075419 (2015).

[33] R. Li, J.-F. Liu, and J. Wang, Strain-modulated perfect valley precession and valley transistor in graphene, Phys. Rev. Appl. **19**, 024075 (2023).

[34] M. A. Mojarro, V. G. Ibarra-Sierra, J. C. Sandoval-Santana, R. Carrillo-Bastos, and G. G. Naumis, Dynamical Floquet spectrum of Kekulé-distorted graphene under normal incidence of electromagnetic radiation, Phys. Rev. B **102**, 165301 (2020).

[35] C. Bao, H. Zhang, X. Wu, S. Zhou, Q. Li, P. Yu, J. Li, W. Duan, and S. Zhou, Coexistence of extended flat band and Kekulé order in Li-intercalated graphene, Phys. Rev. B **105**, L161106 (2022).

[36] C. Bao, H. Zhang, T. Zhang, X. Wu, L. Luo, S. Zhou, Q. Li, Y. Hou, W. Yao, L. Liu, P. Yu, J. Li, W. Duan, H. Yao, Y. Wang, and S. Zhou, Experimental evidence of chiral symmetry breaking in Kekulé-ordered graphene, Phys. Rev. Lett. **126**, 206804 (2021).

[37] S. G. y. García, T. Stegmann, and Y. Betancur-Ocampo, Generalized Hamiltonian for Kekulé graphene and the emergence of valley-cooperative Klein tunneling, Phys. Rev. B **105**, 125139 (2022).

[38] W. Zeng and R. Shen, Enhanced Andreev reflection in Kekulé-Y patterned graphene, Phys. Rev. B **104**, 075436 (2021).

[39] E. Andrade, R. Carrillo-Bastos, M. M. Asmar, and G. G. Naumis, Kekulé-induced valley birefringence and skew scattering in graphene, Phys. Rev. B **106**, 195413 (2022).

[40] E. Andrade, R. Carrillo-Bastos, and G. G. Naumis, Valley engineering by strain in Kekulé-distorted graphene, Phys. Rev. B **99**, 035411 (2019).

[41] Z. Lin, W. Qin, J. Zeng, W. Chen, P. Cui, J.-H. Cho, Z. Qiao, and Z. Zhang, Competing gap opening mechanisms of monolayer graphene and graphene nanoribbons on strong topological insulators, Nano Lett. **17**, 4013 (2017).

[42] S.-H. Lee, H.-J. Chung, J. Heo, H. Yang, J. Shin, U.-I. Chung, and S. Seo, Band gap opening by two-dimensional manifestation of Peierls instability in graphene, ACS Nano **5**, 2964 (2011).

[43] D. L. Bergman, Realization of a vortex in the Kekulé texture of molecular graphene at a Y junction where three domains meet, Phys. Rev. B **87**, 035422 (2013).

[44] C.-Y. Hou, C. Chamon, and C. Mudry, Electron fractionalization in two-dimensional graphenelike structures, Phys. Rev. Lett. **98**, 186809 (2007).

[45] C. Xia, S. Watcharinyanon, A. A. Zakharov, R. Yakimova, L. Hultman, L. I. Johansson, and C. Virojanadara, Si intercalation/deintercalation of graphene on 6*H*-SiC(0001), Phys. Rev. B **85**, 045418 (2012).

[46] S. Watcharinyanon, L. I. Johansson, C. Xia, and C. Virojanadara, Changes in structural and electronic properties of graphene grown on 6*H*-SiC(0001) induced by Na deposition, J. Appl. Phys. **111**, 083711 (2012).

[47] S. Forti and U. Starke, Epitaxial graphene on SiC: From carrier density engineering to quasi-free standing graphene by atomic intercalation, J. Phys. D: Appl. Phys. **47**, 094013 (2014).

[48] F. de Juan, Non-Abelian gauge fields and quadratic band touching in molecular graphene, Phys. Rev. B **87**, 125419 (2013).

[49] W. Han, R. K. Kawakami, M. Gmitra, and J. Fabian, Graphene spintronics, Nat. Nanotechnol. **9**, 794 (2014).

[50] K. K. Gomes, W. Mar, W. Ko, F. Guinea, and H. C. Manoharan, Designer Dirac fermions and topological phases in molecular graphene, Nature (London) **483**, 306 (2012).

[51] C. Gutierrez, C.-J. Kim, L. Brown, T. Schiros, D. Nordlund, E. B. Lochocki, K. M. Shen, J. Park, and A. N. Pasupathy, Imaging chiral symmetry breaking from Kekulé bond order in graphene, Nat. Phys. **12**, 950 (2016).

[52] D. Eom and J.-Y. Koo, Direct measurement of strain-driven Kekulé distortion in graphene and its electronic properties, Nanoscale **12**, 19604 (2020).

[53] Y.-J. Wei, H.-L. Liu, J. Wang, and J.-F. Liu, Supercurrent rectification effect in graphene-based Josephson junctions, Phys. Rev. B **106**, 165419 (2022).

[54] J. J. Wang, S. Liu, J. Wang, and J.-F. Liu, Valley supercurrent in the Kekulé graphene superlattice heterojunction, Phys. Rev. B **101**, 245428 (2020).

[55] C. W. J. Beenakker, N. V. Gnezdilov, E. Dresselhaus, V. P. Ostroukh, Y. Herasymenko, I. Adagideli, and J. Tworzydło, Valley switch in a graphene superlattice due to pseudo-Andreev reflection, Phys. Rev. B **97**, 241403(R) (2018).

[56] J. Wang and S. Fischer, Topological valley resonance effect in graphene, Phys. Rev. B **89**, 245421 (2014).

[57] A. Pachoud, A. Ferreira, B. Özyilmaz, and A. H. Castro Neto, Scattering theory of spin-orbit active adatoms on graphene, Phys. Rev. B **90**, 035444 (2014).

[58] T. Iadecola, D. Campbell, C. Chamon, C.-Y. Hou, R. Jackiw, S.-Y. Pi, and S. V. Kusminskiy, Materials design from nonequilibrium steady states: Driven graphene as a tunable semiconductor with topological properties, Phys. Rev. Lett. **110**, 176603 (2013).

[59] J. W. F. Venderbos, M. Manzardo, D. V. Efremov, J. van den Brink, and C. Ortix, Engineering interaction-induced topological insulators in a $\sqrt{3} \times \sqrt{3}$ substrate-induced honeycomb superlattice, Phys. Rev. B **93**, 045428 (2016).

[60] M. Z. Hasan and C. L. Kane, Colloquium: Topological insulators, Rev. Mod. Phys. **82**, 3045 (2010).

[61] X.-L. Qi and S.-C. Zhang, Topological insulators and superconductors, Rev. Mod. Phys. **83**, 1057 (2011).

[62] D. S. Fisher and P. A. Lee, Relation between conductivity and transmission matrix, Phys. Rev. B **23**, 6851 (1981).

[63] S. K. Wang, J. Wang, and K. S. Chan, Multiple topological interface states in silicene, New J. Phys. **16**, 045015 (2014).

[64] A. Y. Kitaev, Unpaired Majorana fermions in quantum wires, Phys.-Usp. **44**, 131 (2001).